

Review

# Advances in the In Vivo Molecular Imaging of Invasive Aspergillosis

Matthias Gunzer <sup>1,2,\*</sup> , Christopher R. Thornton <sup>3</sup> and Nicolas Beziere <sup>4,\*</sup> 

<sup>1</sup> Institute for Experimental Immunology and Imaging, University Hospital, University Duisburg-Essen, 45147 Essen, Germany

<sup>2</sup> Leibniz-Institut für Analytische Wissenschaften-ISAS-e.V., 44227 Dortmund, Germany

<sup>3</sup> ISCA Diagnostics Ltd. and Biosciences, College of Life & Environmental Sciences, University of Exeter, Exeter EX4 4PY, UK; c.r.thornton@exeter.ac.uk

<sup>4</sup> Werner Siemens Imaging Center, Department of Preclinical Imaging and Radiopharmacy, Eberhard Karls University Tübingen, 72076 Tübingen, Germany

\* Correspondence: matthias.gunzer@uni-due.de (M.G.); nicolas.beziere@med.uni-tuebingen.de (N.B.); Tel.: +49-201-183-6640 (M.G.); +49-7071-29-87511 (N.B.)

Received: 28 October 2020; Accepted: 2 December 2020; Published: 4 December 2020



**Abstract:** Invasive pulmonary aspergillosis (IPA) is a life-threatening infection of immunocompromised patients with *Aspergillus fumigatus*, a ubiquitous environmental mould. While there are numerous functioning antifungal therapies, their high cost, substantial side effects and fear of overt resistance development preclude permanent prophylactic medication of risk-patients. Hence, a fast and definitive diagnosis of IPA is desirable, to quickly identify those patients that really require aggressive antimycotic treatment and to follow the course of the therapeutic intervention. However, despite decades of research into this issue, such a diagnostic procedure is still not available. Here, we discuss the array of currently available methods for IPA detection and their limits. We then show that molecular imaging using positron emission tomography (PET) combined with morphological computed tomography or magnetic imaging is highly promising to become a future non-invasive approach for IPA diagnosis and therapy monitoring, albeit still requiring thorough validation and relying on further acceptance and dissemination of the approach. Thereby, our approach using the *A. fumigatus*-specific humanized monoclonal antibody hJF5 labelled with <sup>64</sup>Cu as PET-tracer has proven highly effective in pre-clinical models and hence bears high potential for human application.

**Keywords:** *Aspergillus fumigatus*; invasive pulmonary aspergillosis; aspergillosis; imaging; positron emission tomography; immunoPET; siderophores; radiolabel

## 1. *Aspergillus fumigatus* and Invasive Pulmonary Aspergillosis

*Aspergillus fumigatus* (*A. fumigatus*) is an ubiquitous saprotrophic mould, whose air-borne spores are routinely inhaled [1], and with DNA of the pathogen detectable in bronchoalveolar lavage (BAL) specimens from healthy individuals [2]. Exposure of humans to *A. fumigatus* can result in a number of different syndromes depending on the extent of the host's immune response. These syndromes range from hypersensitivity/allergy-associated diseases such as allergic bronchopulmonary aspergillosis (ABPA) in immunocompetent individuals to severe invasive disease (invasive pulmonary aspergillosis, IPA) under conditions of severe immunodeficiency [1]. Until the turn of the century, IPA was mainly seen in neutropenic patients, where it was (and remains) the principal life-threatening mould infection of immunocompromised individuals. However, the populations of patients at-risk for the disease have expanded dramatically with the advent of modern tumour therapies such as small molecule kinase inhibitors or chimeric antigen receptor (CAR) T cells, as well as aggressive treatment for

graft-versus-host-disease (GVHD) using high-dose corticosteroids [1]. In the case of CAR T cell therapy, the often-required aggressive management of side effects such as cytokine release syndrome or also the lymphodepletion therapy applied before infusion of CARs do render patients highly susceptible to infections including invasive fungal diseases [3]. In addition, severe viral infections of the lung such as influenza [4] or COVID-19 have led to the emergence of life-threatening co-infections with *A. fumigatus* in otherwise immunocompetent individuals [5,6].

## 2. Clinical Diagnosis of IPA

While effective antifungal drugs are available in the clinic, growing azole resistance in clinical strains of *A. fumigatus* is a serious issue for the successful treatment of IPA [7–9]. However, with a number of new mould-active compounds on the horizon<sup>8</sup>, treatment per se is arguably not the most pressing issue in disease management. Rather, it is our failure to accurately and rapidly diagnose the disease that is driving sub-optimal therapy<sup>1</sup>. Most recent consensus definitions list a number of diagnostic procedures that are required for definitive identification of IPA. Among them are PCR (also combined with DNA sequencing for species determination), high resolution computed tomography (CT), and galactomannan testing of the peripheral blood or BAL recovered during invasive bronchoscopy. Due to its ease-of-use, throughput, low cost and relative patient comfort, CT has proven to be the preferred method for patient screening and the only imaging method recommended for IPA diagnosis. In addition, histological identification of fungal elements in invasive lung biopsies or fungal culture from blood are considered relevant [10]. However, abnormalities in a chest-CT that might indicate IPA are highly variable and by no means specific, making a definitive diagnosis extremely difficult. Furthermore, the growing numbers of non-neutropenic patients suffering from IPA require adjustments to the existing diagnostic paradigms, since established criteria for neutropenic patients are not necessarily translatable to other patient groups [1]. Galactomannan, the predicate microbiological indicator of IPA, is also problematic in patients receiving prophylactic antifungal treatment and which, along with culture, suffers from slow turnaround times in many centres. Consequently, despite substantial progress in IPA detection, there is still no single gold-standard test for the disease that provides high degrees of sensitivity and specificity, and which is non-invasive. As a result, febrile patients with a fever of unknown origin (FUO) are typically treated empirically first with antibiotics and, in the case of persistent fever and neutropenia, with antifungal therapy some days later [11,12].

## 3. Molecular Imaging as an Add-On to Classical Radiology

Molecular imaging aims to circumvent the limitations of classical, purely anatomical, radiological techniques (X-ray, CT, MRI) by providing information based on signals emitted by reporting agents bound to a tracer (e.g., glucose absorbed by metabolically active tissue) or targeting molecule (e.g., a small molecule or antibody binding specifically to a receptor), with specific biological and pharmacokinetic profiles and binding characteristics [13]. Through high contrast delivered by the reporting agent, these techniques can provide information directly correlated to the patho-physiological state of the organism at the molecular level, information that is not obtainable by anatomical data alone [14]. Currently, two main forms of molecular imaging are used: first, optical imaging, relying on the detection of photons emitted by a luminescent or fluorescent reporter [15]; second, radiation-based imaging, relying on the emission of either positrons ( $\beta^+$ ) [16,17] or  $\gamma$ -rays [18,19] from radioactive isotopes. All of these different reporter types have been investigated in relation to IPA in order to develop tools for both researchers and clinicians to diagnose and study *Aspergillus* infection and to monitor therapeutic interventions in vivo. These approaches to imaging IPA will be reviewed in this article.

#### 4. Optical Imaging Enabled by Genetically Modified *Aspergillus* Species

Optical imaging of infections in general, and IPA in particular, stem from three different approaches. First, bioluminescent imaging, based on the autonomous generation of light from luciferin oxidation by the luciferase enzyme [20]. This has been enabled for *Aspergillus* species by inclusion of the luciferase gene into the genome of *A. fumigatus* under the promoter *gpdA* [21]. This tool has been mostly used for monitoring the growth and therapeutic response of *A. fumigatus* infection in vitro and in vivo in animal models, with good sensitivity and high specificity [21–24] as shown in Figure 1, and could be further enhanced by the use of MRI in multimodal environments [25]. However, the bioluminescent approach is limited not only by the need for luciferin injection but also by the requirement for genetically modified strains, thus restricting bioluminescent imaging to the pre-clinical setting with no possibility for clinical translation.

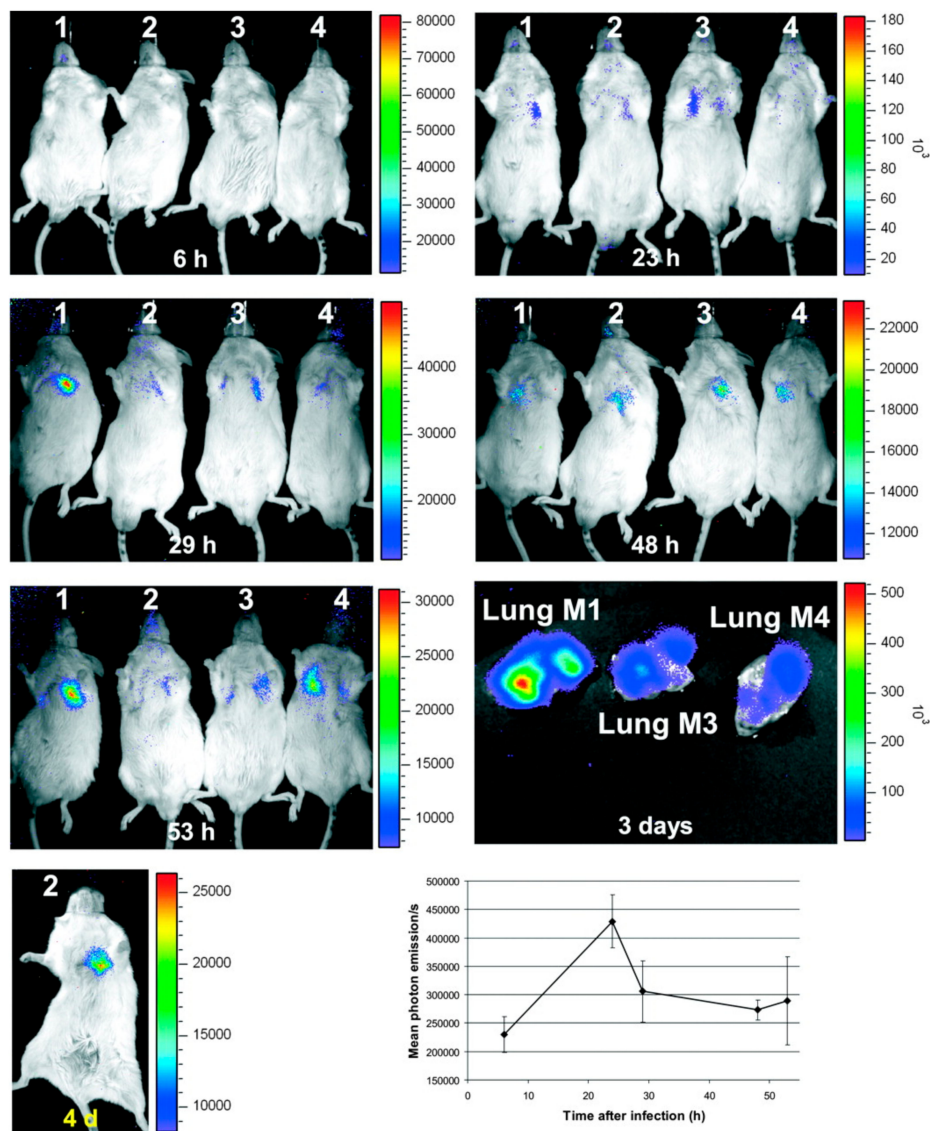


**Figure 1.** Bioluminescence imaging of aspergillosis. Evolution of luminescence emission from BALB/c mice after intra-nasal infection with  $2 \times 10^6$  conidia of bioluminescent *A. fumigatus*. Emission of light peaked 23 h after injection before declining continuously until sacrifice. Ex vivo images were obtained directly after the last in vivo time point. The lower right graph shows the mean signal from the chest of mice through the experiment. Adapted with permission from Brock et al., *Appl. Environ. Microb.* 2008, 74, 7023–7035.

The first limitation, namely injection of an exogenous compound, has been circumvented by the tailoring of fluorescent strains of *Aspergillus* expressing various fluorescent proteins such as the green fluorescent protein [26]. While the inherent limitations of macroscopic optical imaging (especially penetration depth and low resolution in vivo) have a strong influence on the outcome of the experiments, some interesting results have been produced in vitro, notably on the interaction between *A. fumigatus* and phagocytic and non-phagocytic cells [26]. Other fluorescent variants (fluorescent at other wavelengths) have also been obtained for similar purposes [27]. These investigations were expanded upon by the introduction of red-shifted FLuorescent *Aspergillus* REporter (FLARE) [28], red fluorophore (DsRed)-expressing *Aspergillus* conidia additionally grafted with a fluorophore on its surface, allowing for fungal viability and integrity studies in vivo and thus the interaction of the fungus with the host [29,30]. This new variant enabled several additional pre-clinical studies in vitro and in vivo (reviewed elsewhere [31]) and is still actively used, including its evolution—Mitochondria and FLuorescence *Aspergillus* REporter (MitoFLARE)—that allows real-time investigation of granulocyte killing efficiency on *A. fumigatus* in vitro [32]. Further refinement and use of fluorescent strains, combined with technological advances, have allowed a closer look into IPA and notably of host-*Aspergillus* interactions, for example using endoscopy to visualize host responses in situ and in vivo [33]. Collectively, while remaining highly valuable tools for a better understanding of IPA in pre-clinical settings, genetically modified *Aspergillus* strains cannot provide any direct clinical benefits.

## 5. Scintigraphy and SPECT Imaging of Fungal Infections

Scintigraphy and Single photon emission computed tomography (SPECT) rely on the emission of  $\gamma$ -rays from radiotracers such as  $^{99m}\text{Tc}$ ,  $^{111}\text{In}$  or  $^{123}\text{I}$ . The detection of  $\gamma$ -rays by the scintillators, rotated around the sample in the case of SPECT, yield an image of the distribution of the radiotracer in space [18]. In itself, a SPECT image does not contain anatomical information. Hence, a simultaneous CT scan to obtain anatomical information is often performed, providing a reference to locate the radiotracer in the organism. Functional radiotracers require the attachment of  $\gamma$ -ray emitting isotopes onto a chemically modified targeting vector or tracer. In order to provide specificity to the infection site in fungal disease imaging, two main routes have been investigated: radiolabelling of antifungal drugs and radiolabelling of antifungal peptides. More specifically, radiolabelling of the azole antifungal Fluconazole by  $^{99m}\text{Tc}$  ( $^{99m}\text{Tc}$ -Fluconazole) showed increased accumulation at sites of candidiasis (disseminated disease caused by the yeast pathogen *Candida albicans*), but not in bacterial infection or during sterile inflammation [34]. Unfortunately,  $^{99m}\text{Tc}$ -Fluconazole showed no specific accumulation during *A. fumigatus* infection, which was not totally unexpected given the poor efficiency of the drug against IPA. A similar approach was used with the polyene antifungal drug Amphotericin B, also using  $^{99m}\text{Tc}$  as a radiolabel [35], showing promising results with specific accumulation in mould pathogens in in vitro culture models. While these results still require confirmation in vivo, it is foreseeable that the specificity of this radiotracer will be limited to all species sensitive to Amphotericin B and will thus not be *Aspergillus*-specific. A parallel approach focused on improving the delivery of drugs to IPA nodules has highlighted the potential of novel formulations (namely poly(lactide-co-glycolic acid) nanoparticles containing Voriconazole) used in inhalators to deliver drugs efficiently to infected lungs [36]. Radiolabelling of such particles by  $^{99m}\text{Tc}$  could show their accumulation in various major organs as well as increased accumulation and retention in diseased lungs, which could represent a new theranostic approach. However, as with other drug-based approaches, the specificity toward *Aspergillus* species cannot be guaranteed, and accumulation in other types of infections is highly likely.

In addition to small molecular antifungal drugs being radiolabelled, the same approach was applied to anti-microbial peptides [37] such as ubiquicidin [38] and lactoferrin [39] which exhibit antifungal activity against several genera including *Candida* and *Aspergillus*. Here as well,  $^{99m}\text{Tc}$  has been the radioisotope of choice due to the chemical ease with which a suitable chelator can be attached to the antibiotic peptides [40]. The resulting radiolabelled peptides,  $^{99m}\text{Tc}$ -lactoferrin and  $^{99m}\text{Tc}$ -ubiquicidin, have shown interesting profiles for imaging of candidiasis, IPA and bacterial

disease [41], although with no particular specificity. The potential of  $^{99m}\text{Tc}$ -ubiquicidin for fungal infection in particular has been investigated in clinical trials over a 10-year period, and has shown promising results in infection diagnosis and site mapping, although with no specificity towards IPA, as reviewed elsewhere [42].

In between the synthetic drug and the natural peptide pathway, specific targeting vectors have been developed and radiolabelled as candidates for specific imaging of various infections. Short cyclic peptides in particular show interesting pharmacokinetic and targeting potentials and have thus been of interest for detecting IPA.  $^{111}\text{In}$  was used to radiolabel c(CGRLGPFC) [41,43,44], which has shown specific accumulation in the lungs of mice suffering from IPA as seen in Figure 2. Additional work on the same compound revealed the absence of accumulation of the radiotracer in *Geosmithia infections* [45]. Further work is needed to completely validate the specificity of the radiotracer towards *A. fumigatus*, which would then justify first-in-man studies.

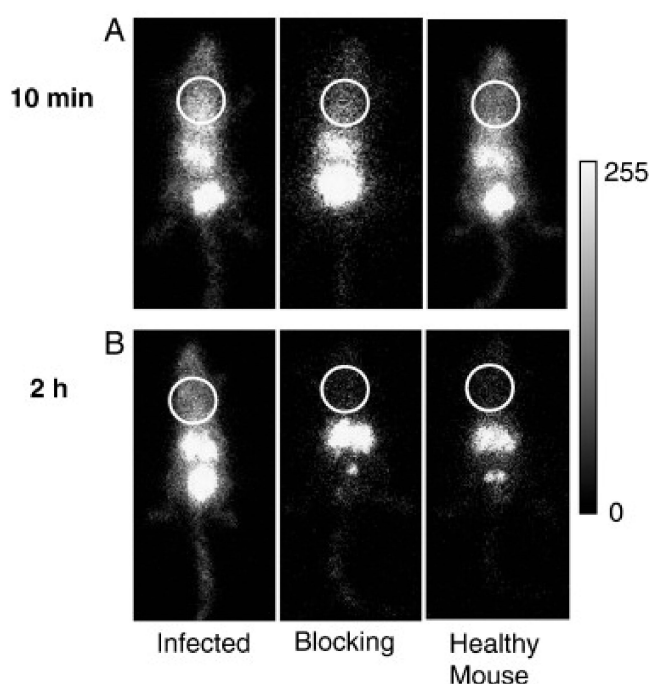


**Figure 2.** Preclinical  $\gamma$ -scintigraphic imaging of aspergillosis. Images of an infected mouse, a mouse co-injected with unlabelled peptide and a healthy control mouse, acquired (A) 10 min and (B) 2 h after intravenous injection of  $^{111}\text{In}$ -DTPA-c(CGRLGPFC)-NH<sub>2</sub>. Circles indicate the chest area encompassing the lungs. Adapted with permission from Yang et al. *Nucl. Med. Biol.* 2009, 36, 259–266.

## 6. Positron Emission Tomography (PET) Approaches

Unlike SPECT, positron emission tomography (PET) relies on the  $\beta^+$  decay of radioactive isotopes. After an initial energy loss, the emitted positron will then encounter an electron, which will result in an annihilation event emitting two photons in approximately opposite directions with respective energies of 511 keV [46]. Detection of these photons by scintillators under certain conditions (most notably simultaneously) will be registered by the system, allowing for reconstruction of an image representing the distribution of photon-producing events in the sample. Given the negligible ambient  $\beta^+$  background, a PET image can thus be directly correlated with the distribution of the radioisotope in the sample, classically-administered as a radiolabelled metallic complex decorating a large molecule (e.g., a peptide or protein) [17] or a radiolabelled organic small molecule [47]. As the decay time is known for the injected isotopes (with the common isotopes and their half-lives being  $^{11}\text{C}$ ,  $t_{1/2} = 20$  min;  $^{68}\text{Ga}$ ,  $t_{1/2} = 67.7$  min;  $^{18}\text{F}$ ,  $t_{1/2} = 110$  min;  $^{64}\text{Cu}$ ,  $t_{1/2} = 12.7$  h and  $^{89}\text{Zr}$ ,  $t_{1/2} = 78.4$  h), decay-corrected signals give a direct insight into the local concentration and the biological properties of the injected radiotracer.

Since the advent of the first PET system, research of targeted radiotracers has been active in a wide variety of fields, most notably cancer. The most broadly used tracer for PET imaging is  $^{18}\text{F}$ -fluorodeoxyglucose ( $^{18}\text{F}$ -FDG), which is taken up by cells due to the Warburg effect and is the current gold standard to map tumours or their metastases in cancer patients [48] and can be used for brain activity monitoring [49], inflammation and infection [50–52] and in general to monitor (patho)-physiological events with a large cellular glucose uptake.

### 6.1. Glucose Uptake

As a result,  $^{18}\text{F}$ -FDG has been used to monitor infections based on the local increased glucose consumption from both the immune system and proliferating infectious pathogens. Despite the clinical potential of  $^{18}\text{F}$ -FDG for monitoring therapy after diagnosis of fungal infections, as reviewed elsewhere [53], in the case of IPA,  $^{18}\text{F}$ -FDG faces three major limitations as a diagnostic procedure: first, it is not specific for the fungus but rather highlights the immune response to an infection and general cellular activity; second,  $^{18}\text{F}$ -FDG is readily taken up by active muscle cells, providing a variable but significant background signal, notably from the heart [54]; third,  $^{18}\text{F}$ -FDG will provide “false positive” signals as it is enriched by other lung diseases such as lung tumours [55], lung fibrosis [56] and various other ailments [57]. This has been shown in pre-clinical models in several studies, notably by comparing the  $^{18}\text{F}$ -FDG signal in IPA models with other sterile or bacterial infection models, as well as in other fungal infections [58]. In the clinic,  $^{18}\text{F}$ -FDG has been the topic of numerous investigations regarding its potential to support IPA diagnosis [59–62].  $^{18}\text{F}$ -FDG-driven diagnosis has proven an interesting tool for disease management through therapy monitoring or tracking of secondary invasion sites and is starting to find its place alongside CT as a radiological workhorse for IPA diagnosis as can be seen in Figure 3. Its use is undoubtedly aided by its FDA approval, low radiation exposure of patients due to short half-life, and general availability in all centres equipped with PET scanners.



**Figure 3.** Clinical  $^{18}\text{F}$ -FDG PET imaging of an acute myelogenous leukaemia patient diagnosed with pulmonary aspergillosis. Complex heterogeneous lesions can be seen in the lungs. Patient was diagnosed using BAL. Adapted from Ankrah et al. *Eur. J. Nucl. Med. Mol. I* 2019, 46, 174–183.

### 6.2. Radiolabelled Drugs and Metabolic Markers

Despite this, it is evident that  $^{18}\text{F}$ -FDG PET imaging does not provide any information on the type of infection, whether bacterial, viral or fungal, which has highlighted the limits of this approach

in terms of diagnosis and therapy monitoring in the fields of inflammation and infection biology. For this reason, other radiotracers have been developed which aim to distinguish between infectious organisms and host cellular activity. The standard approach remains the radiolabelling of readily available drugs, but the difficulty of the chemistry involved and the lack of disease-specificity render this approach unattractive. Despite these limitations, some interesting results have been published, notably radiolabelling of Fluconazole with  $^{18}\text{F}$ , a similar approach to  $^{99\text{m}}\text{Tc}$  radiolabelling for candidiasis diagnosis [63,64]. Here again, the choice of Fluconazole as a targeting vector limits its applicability to IPA diagnostics. Other approaches have harnessed the requirements of infectious organisms for specific nutrients in an attempt to increase the specificity of the radiotracer towards the cause of the infection, while diminishing the background signal from healthy tissue. Here,  $^{18}\text{F}$ -fluoromaltotriose, targeting the maltodextrin transporter of gram-positive and gram-negative bacterial cells [65] or 2- $^{18}\text{F}$ -fluorodeoxysorbitol [66,67] to image gram-negative bacteria, have been tested. Fungi metabolise maltose and sorbitol differently than bacteria, so the applicability of this approach to fungal imaging is unclear.

### 6.3. Siderophores as Radiometal Chelators

All organisms are strictly dependent on iron, namely  $\text{Fe}^{2+}$  and  $\text{Fe}^{3+}$ , for growth and survival [68–70]. For this reason, tight regulatory mechanisms for iron transport and the control of its oxidative status are active at the cellular and organism level. During an infection, invading microorganisms must take up iron in order to multiply. However, the metal is usually tightly sequestered by the host organism as an anti-infectious strategy [71]. As a result, pathogens have evolved iron “traps” as a way to circumvent the lack of iron during disease propagation. *A. fumigatus* in particular developed two iron scavenging pathways: reductive iron assimilation and siderophore-mediated iron acquisition [72,73]. Both are induced by iron starvation, and the importance of these systems has been shown by genetic de-activation of iron scavenging in in vivo models, although only siderophore biosynthesis appears to be essential to *A. fumigatus* pathogenicity [74]. Siderophores are potent ferric iron chelators and are secreted by most bacterial and fungal pathogens. *A. fumigatus* secretes two cyclic siderophores, fusarinine C (FsC) and its tri-acetylated derivative triacetylfusarinine C (TAFC) [75], which are taken up via siderophore-iron transporters (SITs) after successful chelation of ferric iron. Interestingly, SITs are only present in fungi, and while in certain species SITs can demonstrate substrate-specificity, others can import a broad range of siderophores [76]. For these reasons, building contrast agents or radiotracers around siderophore scaffolds to specifically image infection has been investigated heavily in molecular imaging [77] in both optical imaging [78], using fluorophore conjugation, and PET imaging, using an iron-mimicking radionuclides such as  $^{68}\text{Ga}$  [78–82] or  $^{89}\text{Zr}$  [83]. These radiometals can be readily obtained from a Ge/Ga generator for  $^{68}\text{Ga}$  or are commercially available for  $^{89}\text{Zr}$ . With a  $t_{1/2}$  of 68 min,  $^{68}\text{Ga}$  represents an attractive option for clinical applications as it yields a relatively low radiation burden for the patient, while  $^{89}\text{Zr}$  allows for longer imaging times ( $t_{1/2} = 3.27$  days) at the cost of a higher radiation burden. This approach of radiolabelling siderophores using  $^{68}\text{Ga}$  or  $^{89}\text{Zr}$  have shown promising results in in vivo rat models of IPA in a PET/CT (Figure 4), with high accumulation of the radiotracer in the infected lungs and a renal excretion route alongside high metabolic stability, and no marked accumulation in sterile inflammation or cancer [79,81,84]. However, species-specificity is limited by the choice of siderophore: TAFC-based complexes can be taken up by various other fungal pathogens (such as *Fusarium solani*), but not by other fungi in the same or different genera (*A. terreus*, *A. flavus*, *C. albicans*) or bacteria (*S. aureus*, *Pseudomonas aeruginosa*), despite their clinical importance. As a result, it appears that naturally occurring siderophores lack the specificity required for accurate clinical diagnosis of infectious diseases such as IPA, and chemically engineered siderophores with higher specificity are required to unlock the clinical potential of this approach. Interestingly, chemical approaches including a fluorophore in addition to the radiolabel have been recently published [78] and could represent an approach for initial radiological diagnosis based on PET followed by clinical resection of the fungal mass guided by optical imaging during surgery.

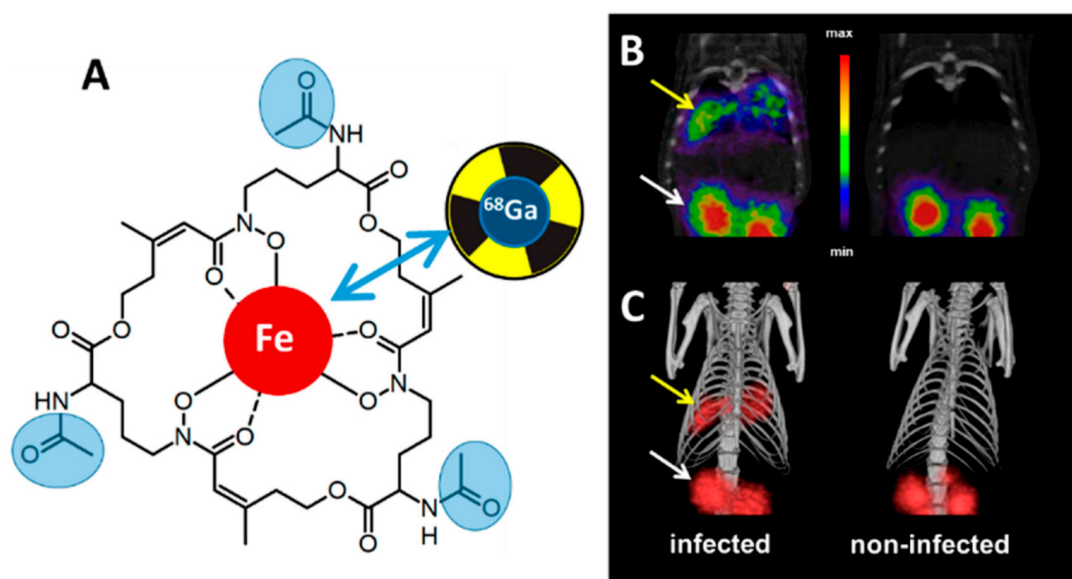


**Figure 4.** Radiolabelled siderophore imaging of Aspergillosis in a rat model. (A) Possible chelation of Fe(III) or  $^{68}\text{Ga}$  by Triacetylfusarinine C (TAFC). Possible chemical modification sites are highlighted in blue. (B)  $\mu\text{PET}/\text{Computed Tomography}$  coronal slices and (C) volume rendered 3D images rat infected by *A. fumigatus* after injection of [ $^{68}\text{Ga}$ ]Ga-TAFC showing accumulation in the lungs (yellow arrow) and excretion through the kidneys (white arrow) of the radiotracer. Adapted from Petrik et al. *J. Fungi* 2020, 6.

#### 6.4. Radiolabelled Antibodies

The use of antibodies able to specifically recognize *Aspergillus* species and to differentiate between actively growing hyphae and inactive spores has recently proved to be a valuable approach for pre-clinical diagnosis of IPA using molecular imaging. The use of radiolabelled antibodies for PET imaging (so called immunoPET [85]) is a relatively new field that has historically focused on oncology, despite its potential for specific diagnosis of different infectious aetiologies that express unique antigens [86]. For IPA specifically, the murine monoclonal antibody (mAb) mJF5 [87] and its humanized counterpart hJF5 [88] have been developed by us. JF5 binds to galactofuranose-rich glycoproteins expressed by the hyphae of all clinically relevant *Aspergillus* species (*A. fumigatus*, *A. terreus*, *A. niger*, *A. flavus* and *A. nidulans*) [89,90] and forms the basis of a novel lateral-flow device (LFD) for IPA detection [87,91,92]. During further investigations by targeted deletion of the gene encoding the enzyme UDP-galactopyranose mutase, JF5 has been shown to bind to the epitope  $\beta$ 1,5-galactofuranose [88]. This epitope is absent in mammals, thus preventing non-specific binding of JF5 to host tissues [93,94]. Radiolabelling of mAb mJF5 with  $^{64}\text{Cu}$  and its use in vivo has demonstrated its ability to differentiate IPA from sterile inflammatory responses or bacterial infections, unlike other approaches published so far. Initially, using mAb mJF5 and the  $^{64}\text{Cu}$  chelator DOTA, we showed markedly increased uptake of the radiotracer in the lungs of *A. fumigatus*-infected animals when compared to healthy animals, but with accompanying uptake of the tracer by the liver [95] (Figure 5). While the high accumulation of the mJF5-based radiotracer in the lungs is directly linked to the presence of invasive hyphae, the liver signal likely resulted from poor stability of the DOTA chelator and/or hepatic clearance of the radiolabelled antibody. Further optimization of the radiotracer in a subsequent study highlighted the benefit of using NODAGA over DOTA as a chelator, leading to improve in vivo stability and enhanced lung targeting [88].

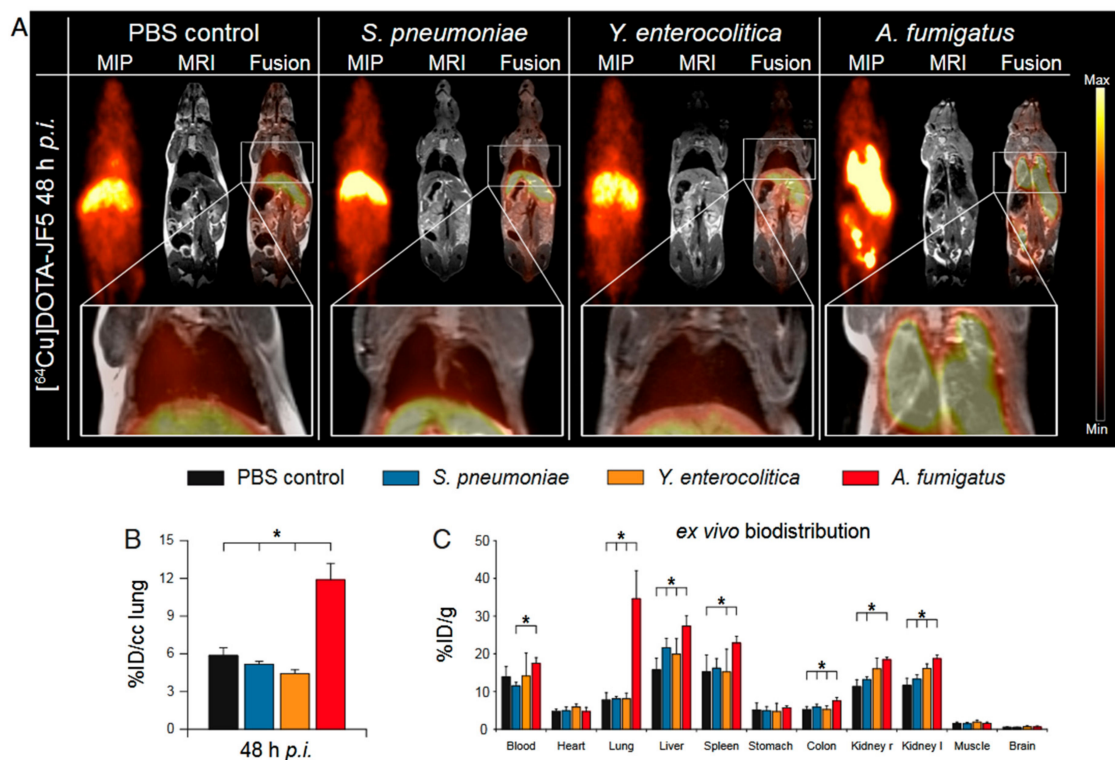


**Figure 5.** Preclinical JF5-based PET imaging of aspergillosis in mice. (A) [<sup>64</sup>Cu]Cu-DOTA-mJF5 PET coronal maximum intensity projection (MIP) and magnetic resonance images (MRI) overlaid (Fusion) in control (PBS inoculated), *S. pneumoniae*, *Y. enterocolitica* and *A. fumigatus* lung infections. Close-up of the lung area in the insert below. (B) Quantification of in vivo radiotracer accumulation in the lungs 48 h post injection (*p.i.*). (C) Quantification of radiotracer bio-distribution ex vivo in excised organs. Data are expressed as the average ± standard deviation of the injected dose (ID), one-way ANOVA, \* *p* < 0.05. Adapted from Rolle et al. *Proc. Natl. Acad. Sci. USA* 2016, 113, E1026–E1033.

The antibody JF5 has been validated for in vitro diagnosis of IPA using bodily fluids (serum or BAL fluid) [87,91,92]. A potential translation of the in vivo PET imaging approach to the clinical setting required humanisation of the antibody. This step was performed using complementarity-determining regions (CDR) grafting of the mouse variable heavy (V<sub>H</sub>) and variable light (V<sub>L</sub>) chain CDRs onto a human IgG1 framework, resulting in the hJF5 antibody that displays improved affinity for the GalF epitope compared to its mouse counterpart [88]. Radiolabelling through NODAGA conjugation and <sup>64</sup>Cu chelation enabled comparative experiments in our neutropenic murine model of IPA. As such, this approach holds enormous promise for specific imaging of IPA in a clinical setting and may even be applicable to other *Aspergillus* diseases such as cerebral aspergillosis, although penetration of the full length antibody into the brain will likely be reliant on disruption of the blood–brain barrier during disease progression [96]. In addition to PET imaging, the JF5 antibody has also very recently been used to obtain high resolution 3D light-sheet fluorescence microscopy images of infected mouse lungs ex vivo by using a fluorophore label, allowing novel insights into different modes of immunosuppression on IPA progression [97].

While currently the only non-invasive IPA-specific imaging procedure, several limitations may hinder the clinical application of radiolabelled hJF5 for PET imaging. Firstly, the pre-clinical models used to test imaging approaches often present a significantly faster disease progression than in humans [98,99]. This limits the window of investigation for the early diagnostic capacity of the imaging method chosen. Secondly, the animal models often rely on complete invasion of the lung by the fungus, whereas the human disease is often represented by nodules of moderate size (a few centimetres) on first appearance of symptoms [100,101]. Lastly, IPA often overlaps with a myriad of other lung diseases

such as chronic obstructive pulmonary disease or cystic fibrosis, co-morbidities that are often difficult to investigate pre-clinically. Notwithstanding these uncertainties, immunoPET imaging based on mAb JF5 represents the most promising candidate for clinical translation to date due to its excellent specificity, overall performance in pre-clinical trials and first-in-human compassionate use which commenced in 2018 with promising preliminary results (unpublished).

## 7. Perspectives

Molecular imaging is showing enormous promise for the clinical diagnosis of IPA [1]. While the more general inflammatory conditions surrounding infections imaged by  $^{18}\text{F}$ -FDG or accumulation of radiolabelled antifungals do not yield the required specificity, siderophore imaging and especially immunoPET have been shown to provide a definitive diagnosis without the need for invasive procedures. Future developments in immunoPET need to address the speed of enrichment in the target tissue and to provide a higher signal-to-noise ratio in acquired images, e.g., by developing smaller targeting vectors such as nanobodies [102]. In any case, the need for rapid and unequivocal diagnosis has lost nothing of its urgency, especially in the current COVID-19 crisis where growing numbers of critically-ill patients are being treated with anti-inflammatory corticosteroids [103], which is opening the door to opportunistic co-infections by *A. fumigatus*.

**Author Contributions:** Conceptualization and writing, M.G., C.R.T. and N.B.; visualization, N.B. All authors have read and agreed to the published version of the manuscript.

**Funding:** This research is funded by the Ministry of Culture and Science of North Rhine-Westphalia, the Governing Mayor of Berlin including Science and Research, and the Federal Ministry of Education and Research (M.G.), the European Union Seventh Framework Programme FP7/2007-2013 under Grant 602820 (M.G., C.R.T., N.B.) and the Werner Siemens Foundation (N.B.).

**Conflicts of Interest:** C.R.T. is director of ISCA Diagnostics Ltd. The funders had no role in the design of the study; in the collection, analyses or interpretation of data; in the writing of the manuscript or in the decision to publish the results.

## References

1. Latge, J.P.; Chamilos, G. Aspergillus fumigatus and Aspergillosis in 2019. *Clin. Microbiol. Rev.* **2019**, *33*. [[CrossRef](#)] [[PubMed](#)]
2. Denning, D.W.; Park, S.; Lass-Flörl, C.; Fraczek, M.G.; Kirwan, M.; Gore, R.; Smith, J.; Bueid, A.; Moore, C.B.; Bowyer, P.; et al. High-frequency triazole resistance found in nonculturable Aspergillus fumigatus from lungs of patients with chronic fungal disease. *Clin. Infect. Dis.* **2011**, *52*, 1123–1129. [[CrossRef](#)] [[PubMed](#)]
3. Hill, J.A.; Li, D.; Hay, K.A.; Green, M.L.; Cherian, S.; Chen, X.; Riddell, S.R.; Maloney, D.G.; Boeckh, M.; Turtle, C.J. Infectious complications of CD19-targeted chimeric antigen receptor-modified T-cell immunotherapy. *Blood* **2018**, *131*, 121–130. [[CrossRef](#)] [[PubMed](#)]
4. Shah, M.M.; Hsiao, E.I.; Kirsch, C.M.; Gohil, A.; Narasimhan, S.; Stevens, D.A. Invasive pulmonary aspergillosis and influenza co-infection in immunocompetent hosts: Case reports and review of the literature. *Diagn. Microbiol. Infect. Dis.* **2018**, *91*, 147–152. [[CrossRef](#)] [[PubMed](#)]
5. Bruno, G.; Fabrizio, C.; Buccoliero, G.B. COVID-19-associated pulmonary aspergillosis: Adding insult to injury. *Lancet Microbe* **2020**, *1*, e106. [[CrossRef](#)]
6. Verweij, P.E.; Gangneux, J.P.; Bassetti, M.; Brüggemann, R.J.M.; Cornely, O.A.; Koehler, P.; Lass-Flörl, C.; van de Veerdonk, F.L.; Chakrabarti, A.; Hoenigl, M.; et al. Diagnosing COVID-19-associated pulmonary aspergillosis. *Lancet Microbe* **2020**, *1*, e53–e55. [[CrossRef](#)]
7. Patterson, T.F.; Thompson, G.R., 3rd; Denning, D.W.; Fishman, J.A.; Hadley, S.; Herbrecht, R.; Kontoyiannis, D.P.; Marr, K.A.; Morrison, V.A.; Nguyen, M.H.; et al. Practice Guidelines for the Diagnosis and Management of Aspergillosis: 2016 Update by the Infectious Diseases Society of America. *Clin. Infect. Dis.* **2016**, *63*, e1–e60. [[CrossRef](#)]
8. Chowdhary, A.; Sharma, C.; Meis, J.F. Azole-Resistant Aspergillosis: Epidemiology, Molecular Mechanisms, and Treatment. *J. Infect. Dis.* **2017**, *216*, S436–S444. [[CrossRef](#)]

9. Verweij, P.E.; Chowdhary, A.; Melchers, W.J.G.; Meis, J.F.; Weinstein, R.A. Azole Resistance in *Aspergillus fumigatus*: Can We Retain the Clinical Use of Mold-Active Antifungal Azoles? *Clin. Infect. Dis.* **2016**, *62*, 362–368. [[CrossRef](#)]
10. Donnelly, J.P.; Chen, S.C.; Kauffman, C.A.; Steinbach, W.J.; Baddley, J.W.; Verweij, P.E.; Clancy, C.J.; Wingard, J.R.; Lockhart, S.R.; Groll, A.H.; et al. Revision and Update of the Consensus Definitions of Invasive Fungal Disease From the European Organization for Research and Treatment of Cancer and the Mycoses Study Group Education and Research Consortium. *Clin. Infect. Dis.* **2020**, *71*, 1367–1376. [[CrossRef](#)]
11. Loizidou, A.; Aoun, M.; Klastersky, J. Fever of unknown origin in cancer patients. *Crit. Rev. Oncol. Hematol.* **2016**, *101*, 125–130. [[CrossRef](#)] [[PubMed](#)]
12. Pizzo, P.A. Management of Patients With Fever and Neutropenia Through the Arc of Time: A Narrative Review. *Ann. Intern. Med.* **2019**, *170*, 389–397. [[CrossRef](#)] [[PubMed](#)]
13. Pysz, M.A.; Gambhir, S.S.; Willmann, J.K. Molecular imaging: Current status and emerging strategies. *Clin. Radiol.* **2010**, *65*, 500–516. [[CrossRef](#)]
14. Anderson, C.J.; Lewis, J.S. Current status and future challenges for molecular imaging. *Philos. Trans. R. Soc. A* **2017**, *375*. [[CrossRef](#)] [[PubMed](#)]
15. Hillman, E.M.C.; Amoozegar, C.B.; Wang, T.; McCaslin, A.F.H.; Bouchard, M.B.; Mansfield, J.; Levenson, R.M. In vivo optical imaging and dynamic contrast methods for biomedical research. *Philos. Trans. R. Soc. A* **2011**, *369*, 4620–4643. [[CrossRef](#)]
16. Vaquero, J.J.; Kinahan, P. Positron Emission Tomography: Current Challenges and Opportunities for Technological Advances in Clinical and Preclinical Imaging Systems. *Annu. Rev. Biomed Eng.* **2015**, *17*, 385–414. [[CrossRef](#)]
17. Brandt, M.; Cardinale, J.; Aulsebrook, M.L.; Gasser, G.; Mindt, T.L. An Overview of PET Radiochemistry, Part 2: Radiometals. *J. Nucl. Med.* **2018**, *59*, 1500–1506. [[CrossRef](#)]
18. Khalil, M.M.; Tremoleda, J.L.; Bayomy, T.B.; Gsell, W. Molecular SPECT Imaging: An Overview. *Int. J. Mol. Imaging* **2011**, *2011*, 1–15. [[CrossRef](#)]
19. Mariani, G.; Bruselli, L.; Kuwert, T.; Kim, E.E.; Flotats, A.; Israel, O.; Dondi, M.; Watanabe, N. A review on the clinical uses of SPECT/CT. *Eur. J. Nucl. Med. Mol. Imaging* **2010**, *37*, 1959–1985. [[CrossRef](#)]
20. Hutchens, M.; Luker, G.D. Applications of bioluminescence imaging to the study of infectious diseases. *Cell. Microbiol.* **2007**, *9*, 2315–2322. [[CrossRef](#)]
21. Brock, M.; Jouvion, G.; Droin-Bergere, S.; Dussurget, O.; Nicola, M.A.; Ibrahim-Granet, O. Bioluminescent *Aspergillus fumigatus*, a New Tool for Drug Efficiency Testing and In Vivo Monitoring of Invasive Aspergillosis. *Appl. Environ. Microbiol.* **2008**, *74*, 7023–7035. [[CrossRef](#)] [[PubMed](#)]
22. Ibrahim-Granet, O.; Jouvion, G.; Hohl, T.M.; Droin-Bergere, S.; Philippart, F.; Kim, O.Y.; Adib-Conquy, M.; Schwendener, R.; Cavaiillon, J.M.; Brock, M. In vivo bioluminescence imaging and histopathologic analysis reveal distinct roles for resident and recruited immune effector cells in defense against invasive aspergillosis. *BMC Microbiol.* **2010**, *10*, 105. [[CrossRef](#)] [[PubMed](#)]
23. Galiger, C.; Brock, M.; Jouvion, G.; Savers, A.; Parlato, M.; Ibrahim-Granet, O. Assessment of Efficacy of Antifungals against *Aspergillus fumigatus*: Value of Real-Time Bioluminescence Imaging. *Antimicrob. Agents Chemother.* **2013**, *57*, 3046–3059. [[CrossRef](#)] [[PubMed](#)]
24. Zeng, Q.Q.; Zhang, Z.; Chen, P.Y.; Long, N.B.; Lu, L.; Sang, H. In vitro and in vivo Efficacy of a Synergistic Combination of Itraconazole and Verapamil Against *Aspergillus fumigatus*. *Front. Microbiol.* **2019**, *10*. [[CrossRef](#)]
25. Poelman, J.; Himmelreich, U.; Vanherp, L.; Zhai, L.C.; Hillen, A.; Holvoet, B.; Belderbos, S.; Brock, M.; Maertens, J.; Vande Velde, G.; et al. A Multimodal Imaging Approach Enables In Vivo Assessment of Antifungal Treatment in a Mouse Model of Invasive Pulmonary Aspergillosis. *Antimicrob. Agents Chemother.* **2018**, *62*. [[CrossRef](#)]
26. Wasylnka, J.A.; Moore, M.M. Uptake of *Aspergillus fumigatus* conidia by phagocytic and nonphagocytic cells in vitro: Quantitation using strains expressing green fluorescent protein. *Infect. Immun.* **2002**, *70*, 3156–3163. [[CrossRef](#)]
27. Szewczyk, E.; Krappmann, S. Conserved Regulators of Mating Are Essential for *Aspergillus fumigatus* Cleistothecium Formation. *Eukaryot. Cell* **2010**, *9*, 774–783. [[CrossRef](#)]

28. Jhingran, A.; Mar, K.B.; Kumasaka, D.K.; Knoblaugh, S.E.; Ngo, L.Y.; Segal, B.H.; Iwakura, Y.; Lowell, C.A.; Hamerman, J.A.; Lin, X.; et al. Tracing Conidial Fate and Measuring Host Cell Antifungal Activity Using a Reporter of Microbial Viability in the Lung. *Cell Rep.* **2012**, *2*, 1762–1773. [[CrossRef](#)]
29. Hickey, P.C.; Read, N.D. Imaging living cells of *Aspergillus* in vitro. *Med. Mycol.* **2009**, *47*, S110–S119. [[CrossRef](#)]
30. Brunel, S.F.; Bain, J.M.; King, J.; Heung, L.J.; Kasahara, S.; Hohl, T.M.; Warris, A. Live Imaging of Antifungal Activity by Human Primary Neutrophils and Monocytes in Response to *A.fumigatus*. *J. Vis. Exp.* **2017**. [[CrossRef](#)]
31. Heung, L.J.; Jhingran, A.; Hohl, T.M. Deploying FLAREs to Visualize Functional Outcomes of Host—Pathogen Encounters. *PLoS Pathog.* **2015**, *11*, e1004912. [[CrossRef](#)] [[PubMed](#)]
32. Ruf, D.; Brantl, V.; Wagener, J. Mitochondrial Fragmentation in *Aspergillus fumigatus* as Early Marker of Granulocyte Killing Activity. *Front. Cell. Infect. Microbiol.* **2018**, *8*. [[CrossRef](#)] [[PubMed](#)]
33. Morisse, H.; Heyman, L.; Salaun, M.; Favennec, L.; Picquenot, J.M.; Bohn, P.; Thiberville, L. In vivo and in situ imaging of experimental invasive pulmonary aspergillosis using fibered confocal fluorescence microscopy. *Med. Mycol.* **2012**, *50*, 386–395. [[CrossRef](#)] [[PubMed](#)]
34. Lupetti, A.; Welling, M.M.; Mazzi, U.; Nibbering, P.H.; Pauwels, E.K.J. Technetium-99m labelled fluconazole and antimicrobial peptides for imaging of *Candida albicans* and *Aspergillus fumigatus* infections. *Eur. J. Nucl. Med. Mol. Imaging* **2002**, *29*, 674–679. [[CrossRef](#)] [[PubMed](#)]
35. Page, L.; Ullmann, A.J.; Schadt, F.; Wurster, S.; Samnick, S. In Vitro Evaluation of Radiolabeled Amphotericin B for Molecular Imaging of Mold Infections. *Antimicrob. Agents Chemother.* **2020**, *64*. [[CrossRef](#)] [[PubMed](#)]
36. Das, P.J.; Paul, P.; Mukherjee, B.; Mazumder, B.; Mondal, L.; Baishya, R.; Debnath, M.C.; Dey, K.S. Pulmonary Delivery of Voriconazole Loaded Nanoparticles Providing a Prolonged Drug Level in Lungs: A Promise for Treating Fungal Infection. *Mol. Pharm.* **2015**, *12*, 2651–2664. [[CrossRef](#)] [[PubMed](#)]
37. Ganz, T.; Lehrer, R.I. Antibiotic peptides from higher eukaryotes: Biology and applications. *Mol. Med. Today* **1999**, *5*, 292–297. [[CrossRef](#)]
38. Hiemstra, P.S.; van den Barselaar, M.T.; Roest, M.; Nibbering, P.H.; van Furth, R. Ubiquicidin, a novel murine microbicidal protein present in the cytosolic fraction of macrophages. *J. Leukoc. Biol.* **1999**, *66*, 423–428. [[CrossRef](#)]
39. Nibbering, P.H.; Ravensbergen, E.; Welling, M.M.; van Berkel, L.A.; van Berkel, P.H.C.; Pauwels, E.K.J.; Nuijens, J.H. Human lactoferrin and peptides derived from its N terminus are highly effective against infections with antibiotic-resistant bacteria. *Infect. Immun.* **2001**, *69*, 1469–1476. [[CrossRef](#)]
40. Blok, D.; Feitsma, R.I.J.; Vermeij, P.; Pauwels, E.J.K. Peptide radiopharmaceuticals in nuclear medicine. *Eur. J. Nucl. Med.* **1999**, *26*, 1511–1519. [[CrossRef](#)]
41. Welling, M.M.; Lupetti, A.; Balter, H.S.; Lanzzeri, S.; Souto, B.; Rey, A.M.; Savio, E.O.; Paulusma-Annema, A.; Pauwels, E.K.J.; Nibbering, P.H. Tc-99m-Labeled antimicrobial peptides for detection of bacterial and *Candida albicans* infections. *J. Nucl. Med.* **2001**, *42*, 788–794. [[PubMed](#)]
42. Ferro-Flores, G.; Avila-Rodriguez, M.A.; Garcia-Perez, F.O. Imaging of bacteria with radiolabeled ubiquicidin by SPECT and PET techniques. *Clin. Transl. Imaging* **2016**, *4*, 175–182. [[CrossRef](#)]
43. Das, S.S.; Wareham, D.W.; Britton, K.E. Tc-99m-labeled antimicrobial peptides for detection of bacterial and *Candida albicans* infections. *J. Nucl. Med.* **2002**, *43*, 1376.
44. Yang, Z.; Kontoyiannis, D.P.; Wen, X.X.; Xiong, C.Y.; Zhang, R.; Albert, N.D.; Li, C. Gamma scintigraphy imaging of murine invasive pulmonary aspergillosis with a In-111-labeled cyclic peptide. *Nucl. Med. Biol.* **2009**, *36*, 259–266. [[CrossRef](#)] [[PubMed](#)]
45. Morisse, H.; Heyman, L.; Salaun, M.; Favennec, L.; Picquenot, J.M.; Bohn, P.; Thiberville, L. In vivo molecular microimaging of pulmonary aspergillosis. *Med. Mycol.* **2013**, *51*, 352–360. [[CrossRef](#)]
46. Pichler, B.J.; Judenhofer, M.S.; Pfannenber, C. Multimodal imaging approaches: PET/CT and PET/MRI. *Handb. Exp. Pharmacol.* **2008**, 109–132.
47. Pichler, V.; Berroteran-Infante, N.; Philippe, C.; Vranka, C.; Klebermass, E.M.; Balber, T.; Pfaff, S.; Nics, L.; Mitterhauser, M.; Wadsak, W. An Overview of PET Radiochemistry, Part 1: The Covalent Labels F-18, C-11, and N-13. *J. Nucl. Med.* **2018**, *59*, 1350–1354. [[CrossRef](#)]
48. Zhu, A.Z.; Lee, D.; Shim, H. Metabolic Positron Emission Tomography Imaging in Cancer Detection and Therapy Response. *Semin. Oncol.* **2011**, *38*, 55–69. [[CrossRef](#)]

49. Verger, A.; Guedj, E. The renaissance of functional F-18-FDG PET brain activation imaging. *Eur. J. Nucl. Med. Mol. Imaging* **2018**, *45*, 2338–2341. [[CrossRef](#)]
50. Treglia, G. Diagnostic Performance of F-18-FDG PET/CT in Infectious and Inflammatory Diseases according to Published Meta-Analyses. *Contrast Media Mol. Imaging* **2019**, *2019*. [[CrossRef](#)]
51. Kung, B.T.; Seraj, S.M.; Zadeh, M.Z.; Rojulpote, C.; Kotheekar, E.; Ayubcha, C.; Ng, K.S.; Ng, K.K.; Au-Yong, T.K.; Werner, T.J.; et al. An update on the role of F-18-FDG-PET/CT in major infectious and inflammatory diseases. *Am. J. Nucl. Med. Mol.* **2019**, *9*, 255–273.
52. Li, Y.M.; Wang, Q.; Wang, X.M.; Li, X.N.; Wu, H.; Wang, Q.S.; Yao, Z.M.; Miao, W.B.; Zhu, X.H.; Hua, F.C.; et al. Expert Consensus on clinical application of FDG PET/CT in infection and inflammation. *Ann. Nucl. Med.* **2020**, *34*, 369–376. [[CrossRef](#)] [[PubMed](#)]
53. Weinstein, E.A.; Ordonez, A.A.; DeMarco, V.P.; Murawski, A.M.; Pokkali, S.; MacDonald, E.M.; Klunk, M.; Mease, R.C.; Pomper, M.G.; Jain, S.K. Imaging Enterobacteriaceae infection in vivo with F-18-fluorodeoxyisobutyl positron emission tomography. *Sci. Transl. Med.* **2014**, *6*. [[CrossRef](#)] [[PubMed](#)]
54. Gupta, K.; Jadhav, R.; Prasad, R.; Virmani, S. Cardiac uptake patterns in routine 18F-FDG PET-CT scans: A pictorial review. *J. Nucl. Cardiol.* **2020**, *27*, 1296–1305. [[CrossRef](#)] [[PubMed](#)]
55. Ambrosini, V.; Nicolini, S.; Caroli, P.; Nanni, C.; Massaro, A.; Marzola, M.C.; Rubello, D.; Fanti, S. PET/CT imaging in different types of lung cancer: An overview. *Eur. J. Radiol.* **2012**, *81*, 988–1001. [[CrossRef](#)]
56. Ko, U.W.; Yoon, H.-y.; Lee, S.H.; Ha, S.; Lee, J.; Kim, D.S.; Ryu, J.-S.; Song, J.W. The Value of 18F-FDG PET/CT in evaluating disease severity in idiopathic pulmonary fibrosis. *Eur. Respir. J.* **2017**, *50*, PA850. [[CrossRef](#)]
57. Capitano, S.; Nordin, A.J.; Noraini, A.R.; Rossetti, C. PET/CT in nononcological lung diseases: Current applications and future perspectives. *Eur. Respir. Rev.* **2016**, *25*, 247–258. [[CrossRef](#)]
58. Sharma, P.; Mukherjee, A.; Karunanithi, S.; Bal, C.; Kumar, R. Potential Role of 18F-FDG PET/CT in Patients With Fungal Infections. *Am. J. Roentgenol.* **2014**, *203*, 180–189. [[CrossRef](#)]
59. Hot, A.; Maunoury, C.; Poiree, S.; Lanternier, F.; Viard, J.P.; Loulergue, P.; Coignard, H.; Bougnoux, M.E.; Suarez, F.; Rubio, M.T.; et al. Diagnostic contribution of positron emission tomography with [<sup>18</sup>F]fluorodeoxyglucose for invasive fungal infections. *Clin. Microbiol. Infect.* **2011**, *17*, 409–417. [[CrossRef](#)]
60. Leroy-Freschini, B.; Treglia, G.; Argemi, X.; Bund, C.; Kessler, R.; Herbrecht, R.; Imperiale, A. 18F-FDG PET/CT for invasive fungal infection in immunocompromised patients. *QJM Int. J. Med.* **2018**, *111*, 613–622. [[CrossRef](#)]
61. Ichiya, Y.; Kuwabara, Y.; Sasaki, M.; Yoshida, T.; Akashi, Y.; Murayama, S.; Nakamura, K.; Fukumura, T.; Masuda, K. FDG-PET in infectious lesions: The detection and assessment of lesion activity. *Ann. Nucl. Med.* **1996**, *10*, 185–191. [[CrossRef](#)] [[PubMed](#)]
62. Ankrah, A.O.; Span, L.F.R.; Klein, H.C.; de Jong, P.A.; Dierckx, R.A.J.O.; Kwee, T.C.; Sathekge, M.M.; Glaudemans, A.W.J.M. Role of FDG PET/CT in monitoring treatment response in patients with invasive fungal infections. *Eur. J. Nucl. Med. Mol. Imaging* **2019**, *46*, 174–183. [[CrossRef](#)] [[PubMed](#)]
63. Fischman, A.J.; Alpert, N.M.; Livni, E.; Ray, S.; Sinclair, I.; Callahan, R.J.; Correia, J.A.; Webb, D.; Strauss, H.W.; Rubin, R.H. Pharmacokinetics of 18F-labeled fluconazole in healthy human subjects by positron emission tomography. *Antimicrob. Agents Chemother.* **1993**, *37*, 1270–1277. [[CrossRef](#)] [[PubMed](#)]
64. Fischman, A.J.; Alpert, N.M.; Livni, E.; Ray, S.; Sinclair, I.; Elmaleh, D.R.; Weiss, S.; Correia, J.A.; Webb, D.; Liss, R. Pharmacokinetics of 18F-labeled fluconazole in rabbits with candidal infections studied with positron emission tomography. *J. Pharmacol. Exp. Ther.* **1991**, *259*, 1351–1359.
65. Gowrishankar, G.; Hardy, J.; Wardak, M.; Namavari, M.; Reeves, R.E.; Neofytou, E.; Srinivasan, A.; Wu, J.C.; Contag, C.H.; Gambhir, S.S. Specific Imaging of Bacterial Infection Using 6''-F-18-Fluoromaltotriose: A Second-Generation PET Tracer Targeting the Maltodextrin Transporter in Bacteria. *J. Nucl. Med.* **2017**, *58*, 1679–1684. [[CrossRef](#)]
66. Li, J.L.; Zheng, H.Y.; Fodah, R.; Warawa, J.; Ng, C. Imaging disease progression of bacterial lung infection in mice with 2-[F-18]-fluorodeoxyisobutyl (F-18-FDS). *J. Nucl. Med.* **2015**, *56*, 586.
67. Li, J.L.; Zheng, H.Y.; Fodah, R.; Warawa, J.M.; Ng, C.K. Validation of 2-F-18-Fluorodeoxyisobutyl as a Potential Radiopharmaceutical for Imaging Bacterial Infection in the Lung. *J. Nucl. Med.* **2018**, *59*, 134–139. [[CrossRef](#)]
68. Anderson, G.J.; Vulpe, C.D. Mammalian iron transport. *Cell. Mol. Life Sci.* **2009**, *66*, 3241–3261. [[CrossRef](#)]
69. Guerinot, M.L. Microbial Iron Transport. *Annu. Rev. Microbiol.* **1994**, *48*, 743–772. [[CrossRef](#)]
70. Howard, D.H. Acquisition, transport, and storage of iron by pathogenic fungi. *Clin. Microbiol. Rev.* **1999**, *12*, 394–404. [[CrossRef](#)]

71. Liu, Z.; Petersen, R.; Devireddy, L. Impaired neutrophil function in 24p3 null mice contributes to enhanced susceptibility to bacterial infections. *J. Immunol.* **2013**, *190*, 4692–4706. [[CrossRef](#)] [[PubMed](#)]
72. Schrettl, M.; Bignell, E.; Kragl, C.; Sabiha, Y.; Loss, O.; Eisendle, M.; Wallner, A.; Arst, H.N.; Haynes, K.; Haas, H. Distinct roles for intra- and extracellular siderophores during *Aspergillus fumigatus* infection. *PLoS Pathog.* **2007**, *3*, e128. [[CrossRef](#)]
73. Haas, H. Molecular genetics of fungal siderophore biosynthesis and uptake: The role of siderophores in iron uptake and storage. *Appl. Microbiol. Biotechnol.* **2003**, *62*, 316–330. [[CrossRef](#)]
74. Schrettl, M.; Bignell, E.; Kragl, C.; Joechl, C.; Rogers, T.; Arst, H.N.; Haynes, K.; Haas, H. Siderophore Biosynthesis But Not Reductive Iron Assimilation Is Essential for *Aspergillus fumigatus* Virulence. *J. Exp. Med.* **2004**, *200*, 1213–1219. [[CrossRef](#)]
75. Haas, H. Fungal siderophore metabolism with a focus on *Aspergillus fumigatus*. *Nat. Prod. Rep.* **2014**, *31*, 1266–1276. [[CrossRef](#)] [[PubMed](#)]
76. Winkelmann, G. Specificity of Siderophore Iron Uptake by Fungi. In *Proceedings of the Biological Chemistry of Iron*; Springer: Dordrecht, The Netherlands, 1982; pp. 107–116.
77. Petrik, M.; Zhai, C.; Haas, H.; Decristoforo, C. Siderophores for molecular imaging applications. *Clin. Transl. Imaging* **2017**, *5*, 15–27. [[CrossRef](#)] [[PubMed](#)]
78. Pfister, J.; Summer, D.; Petrik, M.; Khoylou, M.; Lichius, A.; Kaeopookum, P.; Kochinke, L.; Orasch, T.; Haas, H.; Decristoforo, C. Hybrid Imaging of *Aspergillus fumigatus* Pulmonary Infection with Fluorescent, <sup>68</sup>Ga-Labelled Siderophores. *Biomolecules* **2020**, *10*, 168. [[CrossRef](#)] [[PubMed](#)]
79. Petrik, M.; Haas, H.; Dobrozemsky, G.; Lass-Flörl, C.; Helbok, A.; Blatzer, M.; Dietrich, H.; Decristoforo, C. <sup>68</sup>Ga-Siderophores for PET Imaging of Invasive Pulmonary Aspergillosis: Proof of Principle. *J. Nucl. Med.* **2010**, *51*, 639–645. [[CrossRef](#)]
80. Skriba, A.; Pluhacek, T.; Palyzova, A.; Novy, Z.; Lemr, K.; Hajduch, M.; Petrik, M.; Havlicek, V. Early and Non-invasive Diagnosis of Aspergillosis Revealed by Infection Kinetics Monitored in a Rat Model. *Front. Microbiol.* **2018**, *9*, 2356. [[CrossRef](#)]
81. Petrik, M.; Haas, H.; Laverman, P.; Schrettl, M.; Franssen, G.M.; Blatzer, M.; Decristoforo, C. <sup>68</sup>Ga-Triacetylfusarinine C and <sup>68</sup>Ga-Ferrioxamine E for *Aspergillus* Infection Imaging: Uptake Specificity in Various Microorganisms. *Mol. Imaging Biol.* **2013**, *16*, 102–108. [[CrossRef](#)]
82. Kaeopookum, P.; Summer, D.; Pfister, J.; Orasch, T.; Lechner, B.E.; Petrik, M.; Novy, Z.; Matuszczak, B.; Rangger, C.; Haas, H.; et al. Modifying the Siderophore Triacetylfusarinine C for Molecular Imaging of Fungal Infection. *Mol. Imaging Biol.* **2019**, *21*, 1097–1106. [[CrossRef](#)] [[PubMed](#)]
83. Petrik, M.; Zhai, C.Y.; Novy, Z.; Urbanek, L.; Haas, H.; Decristoforo, C. In Vitro and In Vivo Comparison of Selected Ga-68 and Zr-89 Labelled Siderophores. *Mol. Imaging Biol.* **2016**, *18*, 344–352. [[CrossRef](#)] [[PubMed](#)]
84. Petrik, M.; Pfister, J.; Misslinger, M.; Decristoforo, C.; Haas, H. Siderophore-Based Molecular Imaging of Fungal and Bacterial Infections—Current Status and Future Perspectives. *J. Fungi* **2020**, *6*, 73. [[CrossRef](#)] [[PubMed](#)]
85. Wei, W.J.; Rosenkrans, Z.T.; Liu, J.J.; Huang, G.; Luo, Q.Y.; Cai, W.B. ImmunoPET: Concept, Design, and Applications. *Chem. Rev.* **2020**, *120*, 3787–3851. [[CrossRef](#)]
86. Wiehr, S.; Warnke, P.; Rolle, A.M.; Schutz, M.; Oberhettinger, P.; Kohlhofer, U.; Quintanilla-Martinez, L.; Maurer, A.; Thornton, C.; Boschetti, F.; et al. New pathogen-specific immunoPET/MR tracer for molecular imaging of a systemic bacterial infection. *Oncotarget* **2016**, *7*, 10990–11001. [[CrossRef](#)]
87. Thornton, C.R. Development of an immunochromatographic lateral-flow device for rapid serodiagnosis of invasive aspergillosis. *Clin. Vaccine Immunol.* **2008**, *15*, 1095–1105. [[CrossRef](#)]
88. Davies, G.; Rolle, A.M.; Maurer, A.; Spycher, P.R.; Schillinger, C.; Solouk-Saran, D.; Hasenberg, M.; Weski, J.; Fonslet, J.; Dubois, A.; et al. Towards Translational ImmunoPET/MR Imaging of Invasive Pulmonary Aspergillosis: The Humanised Monoclonal Antibody JF5 Detects *Aspergillus* Lung Infections In Vivo. *Theranostics* **2017**, *7*, 3398–3414. [[CrossRef](#)]
89. Thornton, C.R. Breaking the mould—Novel diagnostic and therapeutic strategies for invasive pulmonary aspergillosis in the immune deficient patient. *Expert Rev. Clin. Immunol.* **2014**, *10*, 771–780. [[CrossRef](#)]
90. Latge, J.P. Galactofuranose containing molecules in *Aspergillus fumigatus*. *Med. Mycol.* **2009**, *47*, S104–S109. [[CrossRef](#)]

91. Prattes, J.; Lackner, M.; Eigl, S.; Reischies, F.; Raggam, R.B.; Koidl, C.; Flick, H.; Wurm, R.; Palfner, M.; Wolfler, A.; et al. Diagnostic accuracy of the Aspergillus-specific bronchoalveolar lavage lateral-flow assay in haematological malignancy patients. *Mycoses* **2015**, *58*, 461–469. [[CrossRef](#)]
92. Hoenigl, M.; Eigl, S.; Heldt, S.; Duettmann, W.; Thornton, C.; Prattes, J. Clinical evaluation of the newly formatted lateral-flow device for invasive pulmonary aspergillosis. *Mycoses* **2018**, *61*, 40–43. [[CrossRef](#)] [[PubMed](#)]
93. Schmalhorst, P.S.; Krappmann, S.; Vervecken, W.; Rohde, M.; Muller, M.; Braus, G.H.; Contreras, R.; Braun, A.; Bakker, H.; Routier, F.H. Contribution of galactofuranose to the virulence of the opportunistic pathogen *Aspergillus fumigatus*. *Eukaryot. Cell* **2008**, *7*, 1268–1277. [[CrossRef](#)] [[PubMed](#)]
94. Marino, C.; Rinflerch, A.; de Lederkremer, R.M. Galactofuranose antigens, a target for diagnosis of fungal infections in humans. *Future Sci.* **2017**, *3*. [[CrossRef](#)]
95. Rolle, A.M.; Hasenberg, M.; Thornton, C.R.; Solouk-Saran, D.; Mann, L.; Weski, J.; Maurer, A.; Fischer, E.; Spycher, P.R.; Schibli, R.; et al. ImmunoPET/MR imaging allows specific detection of *Aspergillus fumigatus* lung infection in vivo. *Proc. Natl. Acad. Sci. USA* **2016**, *113*, E1026–E1033. [[CrossRef](#)] [[PubMed](#)]
96. Schwartz, S.; Thiel, E. Cerebral aspergillosis: Tissue penetration is the key. *Med. Mycol.* **2009**, *47*, S387–S393. [[CrossRef](#)]
97. Amich, J.; Mokhtari, Z.; Strobel, M.; Vialetto, E.; Sheta, D.; Yu, Y.D.; Hartweg, J.; Kalleda, N.; Jarick, K.J.; Brede, C.; et al. Three-Dimensional Light Sheet Fluorescence Microscopy of Lungs To Dissect Local Host Immune-*Aspergillus fumigatus* Interactions. *Mbio* **2020**, *11*. [[CrossRef](#)]
98. Desoubeaux, G.; Cray, C. Animal Models of Aspergillosis. *Comp. Med.* **2018**, *68*, 109–123.
99. Desoubeaux, G.; Cray, C. Rodent Models of Invasive Aspergillosis due to *Aspergillus fumigatus*: Still a Long Path toward Standardization. *Front. Microbiol.* **2017**, *8*. [[CrossRef](#)]
100. Kousha, M.; Tadi, R.; Soubani, A.O. Pulmonary aspergillosis: A clinical review. *Eur. Respir. Rev.* **2011**, *20*, 156–174. [[CrossRef](#)]
101. Munoz, P.; Guinea, J.; Bouza, E. Update on invasive aspergillosis: Clinical and diagnostic aspects. *Clin. Microbiol. Infect.* **2006**, *12*, 24–39. [[CrossRef](#)]
102. Rashidian, M.; LaFleur, M.W.; Verschoor, V.L.; Dongre, A.; Zhang, Y.; Nguyen, T.H.; Kolifrath, S.; Aref, A.R.; Lau, C.J.; Paweletz, C.P.; et al. Immuno-PET identifies the myeloid compartment as a key contributor to the outcome of the antitumor response under PD-1 blockade. *Proc. Natl. Acad. Sci. USA* **2019**, *116*, 16971–16980. [[CrossRef](#)] [[PubMed](#)]
103. Apostolopoulou, A.; Esquer Garrigos, Z.; Vijayvargiya, P.; Lerner, A.H.; Farmakiotis, D. Invasive Pulmonary Aspergillosis in Patients with SARS-CoV-2 Infection: A Systematic Review of the Literature. *Diagnostics* **2020**, *10*, 807. [[CrossRef](#)] [[PubMed](#)]

**Publisher’s Note:** MDPI stays neutral with regard to jurisdictional claims in published maps and institutional affiliations.



© 2020 by the authors. Licensee MDPI, Basel, Switzerland. This article is an open access article distributed under the terms and conditions of the Creative Commons Attribution (CC BY) license (<http://creativecommons.org/licenses/by/4.0/>).